Inorganic Chemistry

Article

pubs.acs.org/IC

Homoleptic "Star" Ru(II) Polypyridyl Complexes: Shielded Chromophores to Study Charge-Transfer at the Sensitizer-TiO_2 Interface

Patrik G. Johansson,[‡] Yongyi Zhang,[†] Gerald J. Meyer,*[,‡] and Elena Galoppini*[,†]

[†]Chemistry Department, Rutgers University, 73 Warren Street, Newark, New Jersey 07102, United States

[‡]Department of Chemistry and Material Science & Engineering, John Hopkins University, 3400 North Charles Street, Baltimore, Maryland 21218, United States

Supporting Information

ABSTRACT: Three homoleptic star-shaped ruthenium polypyridyl complexes, termed Star YZ1, Star YZ2, and Star YZ3, where the Ru(II) center is coordinated to three bipyridine ligands each carrying two oligo(phenylene ethynylene) (OPE) rigid linker units terminating with isophthalic ester (Ipa) groups for binding to metal-oxide surfaces were synthesized. In Star YZ3, each OPE linker was substituted with two *n*-butoxy (*n*-BuO) solubilizing groups. Star complex YZ4, which is homoleptic but lacks the octahedral symmetry, was synthesized as a reference compound. The Star complexes were synthesized using two approaches: in the first, $Ru(4,4'\text{-}(Br)_2\text{-}2,2'\text{-bpy})_3$ was reacted in a Sonogashira cross coupling reaction with the ethynyl-OPE-Ipa linkers; in the second, the 2,2′-bpy-OPE-Ipa ligands were reacted with $Ru(DMSO)_4(PF_6)_2$. The photophysical behavior of the Star complexes were studied in fluid solution and anchored to the surface of mesoporous nanocrystalline TiO_2 thin films (Star/TiO_2). To a first approximation the excited state behavior in CH_3CN was unchanged when the compounds were anchored to a TiO_2 thin film, indicating that the highly symmetrical (octahedral) and rigid molecular structure of the ligands shielded the chromophoric core from the TiO_2 semiconductor. Inefficient excited state injection, $\phi_{inj} < 0.05$, was observed to occur on a nanosecond time scale with slow recombination. In addition, the presence of *n*-BuO groups on the linker unit gave a large increase in the extinction coefficient of YZ3, which allows for enhanced harvesting of sunlight. The results indicate that molecular design on the nanometer length scale can be utilized to control excited state relaxation pathways at semiconductor surfaces.

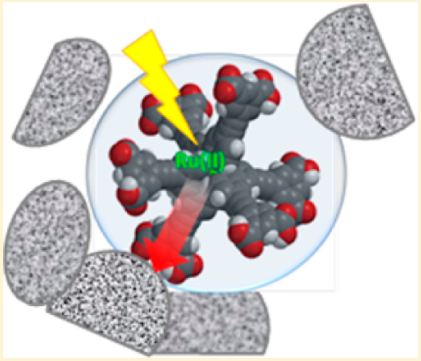

INTRODUCTION

The study of photoinduced electron transfer between Ru-polypyridyl complexes and nanostructured metal oxide (MO) semiconductors is important for the development of photocatalysts and dye sensitized solar cells.[1−3] Numerous sensitizers composed of a Ru(II) coordination compound (or an organic chromophore) with a linker segment terminated with surface anchoring groups have been developed over the past decade as model compounds for interfacial electron transfer studies. Fundamental studies of such sensitizers have led to more efficient devices and to a better understanding of interfacial charge transfer processes.[4−7] An important goal is to control the orientation of the dye-linker-anchor molecule on the MO surface since interfacial heterogeneity of the nanostructured MO films can otherwise prevail, resulting in a broad distribution of molecular orientations. Such disorder can complicate kinetic analysis and decreases our fundamental understanding of electronic processes at the interface. For instance, Willig has shown that complicated charge injection kinetics on nanoparticle mesoporous films is due, at least in part, to surface heterogeneity and that the kinetics were different on single crystal surfaces.[8] More recently, Diau and co-workers found an increased charge recombination rate and lower solar conversion efficiencies in DSSCs with porphyrin-linker-anchor sensitizers as the length of the rigid linker was increased. This behavior was attributed to either the porphyrin unit having a closer proximity to the semiconductor than what would ideally have been expected if the linker was perpendicular to the TiO_2 surface, or by direct contacts with nearby nanocrystallites that the surface anchor groups were not interacting with.[9,10] In a study aimed at probing this effect, we observed that while the linker structure and position of anchor groups can be used to control the binding geometry on planar surfaces, disordered binding is likely to occur on colloidal films.[11]

In this paper we describe homoleptic Ru(II) star complexes which were prepared as part of a strategy aimed at shielding the chromophoric unit from the environment, while providing excellent control over surface binding with a homoleptic ligand design.[12,13] In these nanosized, highly symmetrical star-shaped complexes, the Ru(II) center is coordinated to three identical

Received: February 20, 2013
Published: June 24, 2013

   dx.doi.org/10.1021/ic4004565 | *Inorg. Chem.* 2013, 52, 7947−7957

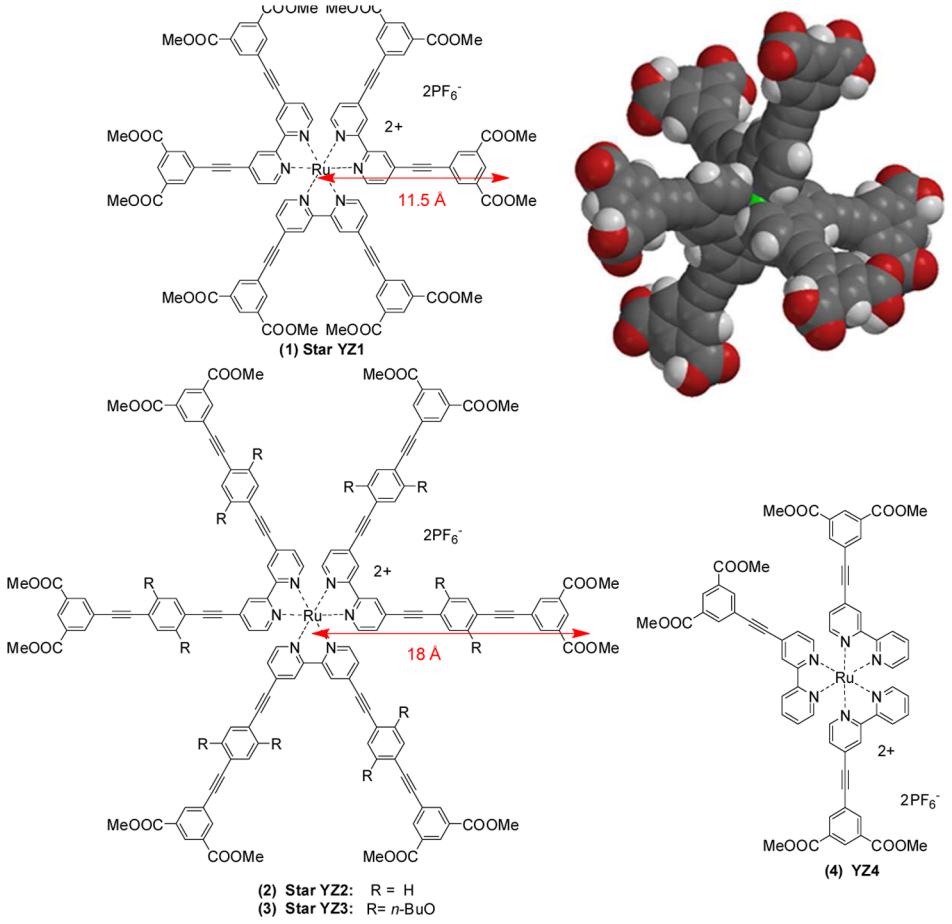

Figure 1. Star complexes YZ1, YZ2, YZ3, and YZ4, and space filling model of Star YZ1. Calculated distances were measured from Ru center to midpoint of ester MeO oxygen in a model calculated using Spartan ′10 (Wave function, Inc.; geometry optimization, MM1).

bipyridine ligands each carrying two oligo (phenylene ethynylene) (OPE) conjugated, rigid linker unit, Star YZ1, Star YZ2, and Star YZ3, shown in Figure 1, terminating with isophthalic esters (Ipa) for binding to metal-oxide surfaces. When these octahedral compounds, having a diameter ranging from 2 to 4 nm, are projected on a plane they resemble a six-pointed star, and are henceforth referred to as Star complexes.

The octahedral symmetry and the long rigid linkers prevent close contact of the $Ru(bpy)_3$ core in the Star complexes with the semiconductor surface. In Star YZ3 each OPE linker was substituted with two *n*-butoxy side chains to improve solubility in organic solvents. Star YZ4 is homoleptic, but lacks the octahedral symmetry of the other Star complexes and hence the chromophoric Ru center is not fully shielded by the linker; it was synthesized to serve as a comparison. The OPE-Ipa bridges of the complexes were identical to those prepared for rigid-rod complexes having the structure $Ru(bpy)_2OPE_n$-Ipa that we had previously studied,[14] to make a comparison between the heteroleptic and the homoleptic design. In a recent communication the initial photophysical studies of Star YZ2 and Star YZ3 in solution and on TiO_2 surfaces were reported.[15] Interestingly, a remarkable enhancement of the extinction coefficient for Star YZ3 was observed in the visible region that was ascribed to the presence of the n-BuO groups.[12,15] In this work we report the synthesis of Stars YZ1, YZ2, YZ3, and YZ4, and the study of their photophysical properties in solution and on metal oxide films. In particular, we wanted to probe how charge transfer is influenced by the bridge length by comparing Star YZ1 with Star YZ2, and study the shielding effect of the homoleptic, octahedral arrangements of the ligands by comparing Star YZ1 with Star YZ4 and with the Ru-rigid rod compounds reported previously.[14]

EXPERIMENTAL SECTION

Measurements. The setup for the steady state and time-resolved spectroscopic measurements,[16] and the preparation of the mesoporous nanocrystallites of TiO_2, anatase ~15 nm in diameter, 10 μm thin films are available in the literature.[17,18] Sensitization was achieved by first base pretreating TiO_2 films at pH 11.1 and then immersing the thin films in micromolar 1:1 (v/v) *n*-butanol: CH_3CN solutions of the star compounds for 24–72 h. The films were then washed thoroughly with CH_3CN and transferred to a standard 1 cm^2 quartz cuvette for characterization. The macroscopic surface coverage, Γ in mol/cm^2, was determined from the measured absorption with a modified Beer–Lambert law Abs $=1000 \times \Gamma \times \varepsilon$, where ε was the molar decadic extinction (absorption) coefficient, M^{-1} cm^{-1}, that was assumed to be the same in solution and on the surface. Unless otherwise specified, all measurements were made in neat CH_3CN at room temperature under argon.

General Procedures. All the air and moisture sensitive reactions were carried out in flame-dried glassware and under nitrogen atmosphere. "Standard workup" in the synthetic procedures refers to the following workup sequence: (1) the aqueous layer was extracted three times with the indicated solvent; (2) the organic layers were collected and dried with anhydrous Na_2SO_4; (c) the solvent was removed in vacuo on a rotary evaporator. Flash column chromatography was performed on silica gel (230–400 mesh), and TLC on

dx.doi.org/10.1021/ic4004565 | Inorg. Chem. 2013, 52, 7947–7957

aluminum-backed silica gel plates. NMR spectra were obtained on a Varian INOVA 500 spectrometer operating at 499.90 MHz for ^{1}H NMR spectra and 124.98 MHz for ^{13}C NMR spectra and collected in $CDCl_3$, unless otherwise specified. The ^{1}H NMR spectra were referenced to tetramethylsilane or the central line of the solvent and the ^{13}C NMR spectra to the central line of the solvent. GC/MS data were obtained on a HP 6890 gas chromatograph equipped with a HP 5973 MS detector and a capillary column (HP 19091s-433:30 m, phenyl methyl siloxane). Major ions were recorded to unit mass, and the intensity was parenthetically indicated as a percentage of the strongest peak. High resolution mass spectra (ESI) were collected on the FTMS departmental facility at Rutgers Newark, equipped with an Apex-ultra 70 hybrid Fourier transform mass spectrometer (Bruker Daltonics). Melting points were measured with a Fisher melting point apparatus.

Fourier-transform infrared attenuated total reflectance (ATR-FTIR) spectra of the dyes neat (powders) and bound to the metal oxide films were collected on a Thermo Electron Corporation Nicolet 6700 FT-IR equipped with a ZnSe crystal. Before every measurement the spectrometer was purged with nitrogen for at least 30 min. For dye molecules the N_2 atmosphere was utilized as the background. For sensitized films, an unsensitized TiO_2 film was used as the background. Between each measurement, the ZnSe crystal was cleaned with methanol or acetone.

Cyclic voltammetry (CV) for solution studies was performed on a BAS CV-50W potentiostat, in tetrabutylammonium hexafluorophosphate acetonitrile (0.26 M) electrolyte. A standard three-electrode arrangement was used, including a glassy carbon electrode (2 mm diameter) as the working electrode, a platinum wire auxiliary electrode, and an Ag/AgCl reference electrode. The sensitizer concentration was about 0.5 mM, and the measurements were carried out at room temperature under nitrogen atmosphere. Ferrocene was used as an internal reference.

Data Fitting. Kinetic data fitting were performed using Origin 7.03 and implementing a least-squares error minimization method, Levenberg–Marquardt iteration. The Franck–Condon (FC) line shape analysis was analyzed and modeled using Wolfram Mathematica 7.0.

Materials. Chloroform, ethyl acetate, and dichloromethane were HPLC grade and used as received. Hexane for column chromatography was distilled. Tetrahydrofuran (THF) was distilled from sodium/benzophenone under nitrogen atmosphere immediately prior to use. Triethylamine, diisopropylamine, benzene, and toluene were distilled from CaH_2 under nitrogen atmosphere prior to use. 1,4-Dibutoxybenzene was purchased from TCI. 4,4′-Bromo-2,2′-bipyridine was purchased from Carbosynth. 2,2′-Bipyridine *N*,*N*′-dioxide, 2,2′-bipyridyl *N*-oxide, dimethyl 5-bromoisophthalate, 1,4-bis-((trimethylsilyl)ethynyl)benzene, trimethylsilylacetylene, and $AgPF_6$ were purchased from Fisher-Acros or from Sigma-Aldrich. All palladium catalysts and $Ru(DMSO)_4Cl_2$ were purchased from Strem and stored at 5–10 °C. Organolithium reagents (MeLi/LiBr, 1.5 M solution in diethyl ether), copper catalysts (CuI and CuBr), tetrabutylammoniumfluoride trihydrate (TBAF), and all other commercially available chemicals were used as received. The following compounds were prepared according to published literature: 4,4′-diiodo-2,2′-bipyridine (**14**),[19,20] dimethyl 5-ethynyl isophthalate (**7**),[21] dimethyl 5((4-ethynylphenyl)ethynyl) isophthalate (**8**),[22] dimethyl 5-(2,2′-bipyridin-4-ylethynyl)isophthalate (**16**),[21] and $Ru(DMSO)_4(PF_6)_2$.[22]

In particular, $Ru(DMSO)_4(PF_6)_2$ was synthesized by refluxing the commercially available $Ru(DMSO)_4Cl_2$ and $AgPF_6$ in ethanol for about 12 h under nitrogen atmosphere, followed by filtration through Celite 521. The resulting orange-yellow $Ru(DMSO)_4(PF_6)_2$, which is a highly hygroscopic solid, was kept under a nitrogen atmosphere and used shortly thereafter.

Synthesis. *Ruthenium Tris(4,4′-dibromo-2,2′-bipyridine) (**6**).* $Ru(DMSO)_4(PF_6)_2$ (0.44 g, 0.58 mmol), 4,4′-dibromo-2,2′-bipyridine (**5**, 0.65 g, 2.03 mmol), THF (5 mL), and nitrogen-purged 1-butanol (30 mL) were added into a round-bottom flask, and the reaction mixture was heated to reflux under nitrogen atmosphere. Every 24 h, the reaction mixture was monitored by UV–vis spectroscopy until the reaction completed. The reaction mixture was cooled to room temperature and filtered. The filtrate was condensed under vacuum, and an orange powder (**6**, 0.3 g; Yield: 48%) formed by adding hexane. ^{1}H NMR (methanol)-d_4: δ 9.04(d, 3 H, J = 1.5 Hz), δ 7.60–7.75(m, 6 H). ^{13}C NMR (methanol)-d_4: δ 158.51, 153.66, 136.33, 132.91, 130.13.

*Star YZ1 (**1**).* A flame-dried round-bottom flask was charged with ruthenium tris(4,4′-dibromo-2,2′-bipyridine) (**6**, 50 mg, 0.038 mmol), benzene (2.5 mL), diisopropylamine (2 mL), THF (2 mL), dimethyl 5-ethynylisophthalate (**7**, 106 mg, 0.486 mmol), and $Pd(PPh_3)_4$ (5 mg, 0.004 mmol). The reaction mixture was stirred at 80 °C under nitrogen atmosphere for 3 days and monitored with TLC. After cooled to room temperature, the reaction mixture was filtered, and the solvent was removed in vacuo. The crude product was purified by silica gel column chromatography (acetonitrile:H_2O, 85:15, v/v) to remove any unreacted starting material. The last band of silica gel was collected and rinsed with THF and acetone to give an orange-red powder (**1**, 40 mg; Yield: 48%). ^{1}H NMR (acetone)-d_6: δ 9.22 (s, 6 H), δ 8.64 (s, 6 H), δ 8.40 (s, 12 H), δ 8.36–8.37 (d, 6 H, J = 6.0 Hz), δ 7.81–7.83 (m, 6 H), δ 3.98 (s, 36 H) ppm. HRMS (ESI) calcd for $C_{102}H_{72}N_6O_{24}Ru^{2+}$: 1866.7897. Found: 1866.3726. The ^{13}C NMR spectrum was not obtained because of the low solubility. IR-ATR (cm^{-1}): 2952 ($C-H_{Ar}$), 2850 ($C-H_{CH3}$), 2218 ($C\equiv C$), 1720 ($C=O$), 1610 ($C=C_{Ar}$), 1479, 1441, 1311, 1249 ($C-O$), 1201, 1159, 995, 916, 879, 842 ($C-H_{Ar}$).

*Star YZ2 (**2**).* A flame-dried round-bottom flask was charged with ruthenium tris(4,4′-dibromo-2,2′-bipyridine) (**6**, 50 mg, 0.038 mmol), benzene (2.5 mL), diisopropylamine (2 mL), THF (4 mL), dimethyl 5-((4-ethynylphenyl)ethynyl)isophthalate (**8**, 0.18 g, 0.460 mmol), and $Pd(PPh_3)_4$ (5 mg, 0.004 mmol). The reaction mixture was stirred at 80 °C under nitrogen atmosphere for 4 days and monitored with TLC. After cooling to room temperature, the reaction mixture was filtered, and the solvent was removed in vacuo. The crude product was purified by silica gel column chromatography (acetonitrile:H_2O, 85:15, v/v) to remove any unreacted starting material. The last band of silica gel was saved and rinsed with THF and acetone to give orange-red powder (**2**, 30 mg; Yield: 30%). ^{1}H NMR (THF)-d_8: δ 8.92(s, 6H), δ 8.60 (broad, 6H), δ 8.36 (s, 12H), δ 8.04–8.06 (m, 6H), δ 7.67 (broad, 30H), δ 3.93 (s, 36H) ppm. HRMS (ESI) calcd for $C_{150}H_{96}N_6O_{24}Ru^{2+}$: 2467.5083. Found: 2467.5768. The ^{13}C NMR is not available because of the low solubility. IR-ATR (cm^{-1}): 2956 ($C-H_{Ar}$), 2858 ($C-H_{CH3}$), 2216 ($C\equiv C$), 1724 ($C=O$), 1600 ($C=C_{Ar}$), 1508, 1459, 1438, 1378, 1351, 1247 ($C-O$), 1120, 1070, 1039, 993, 912, 837 ($C-H_{Ar}$).

*1,4-Dibutoxy-2,5-diiodobenzene (**10**).* A suspension of 1,4-dibutoxybenzene (**9**, 0.89 g, 4 mmol), mercury(II) acetate (3.19 g, 10 mmol) and iodine (2.54 g, 10 mmol) in CH_2Cl_2 (70 mL) was kept stirring overnight at room temperature. The mixture was filtered through Celite 521 and the filtrate was washed with $Na_2S_2O_{3\ aq}$ (10%), $NaHSO_{3\ aq}$ (20%), H_2O, and $NaCl_{\ aq}$ (10%). After drying over Na_2SO_4, the organic solvent was evaporated in vacuo. The crude product was triturated with ethanol to give product **10** (1.73 g; Yield: 77%). ^{1}H NMR ($CDCl_3$): δ 7.18 (s, 2H), δ 3.92–3.95 (t, 4H, J = 6.5 Hz), δ 1.76–1.81 (m, 4H), δ 1.50–1.57 (m, 4H), δ 0.97–1.00 (t, 6H, J = 7.0 Hz) ppm. ^{13}C NMR ($CDCl_3$): δ 152.77, 122.69, 86.27, 69.96, 31.18, 19.25, 13.79. HRMS (ESI) calcd for $C_{14}H_{20}I_2O_2$: 474.1163. Found: 473.3399(M-H).

*((2,5-Dibutoxy-4-iodophenyl)ethynyl)trimethyl Silane (**11**).* A flame-dried round-bottom flask was charged with 1,4-dibutoxy-2,5-diiodobenzene (**10**, 6.0 g, 12.66 mmol), diisopropylamine (35 mL), THF (85 mL), CuI (0.12 g, 0.633 mmol), trimethylsilylacetylene (1.75 mL, 12.66 mmol), and $Pd(PPh_3)_2Cl_2$ (0.89 g, 1.266 mmol). Trimethylsilylacetylene was diluted with THF (15 mL) and was added to the reaction mixture dropwise. The reaction mixture was kept stirring overnight at room temperature under nitrogen atmosphere, then filtered, and the solvent was removed in vacuo. After standard workup with $CHCl_3$, the remaining crude product was purified by silica gel column chromatography ($CHCl_3$:hexane, 1:4, v/v) to give product **11** (2.3 g; Yield: 41%) as a pale yellow oil. ^{1}H NMR

dx.doi.org/10.1021/ic4004565 | Inorg. Chem. 2013, 52, 7947–7957

((acetone)-d_6): δ 7.40 (s, 1H), δ 6.92 (s, 1H), δ 3.98−4.03 (ddd, 4H, J = 1.5, 6.5 Hz), δ 1.72−1.80 (m, 4H), δ 1.52−1.60 (m, 4H), δ 0.96−0.99 (t, 6H, J = 7.0 Hz), δ 0.22 (s, 9H) ppm. ^{13}C NMR ($CDCl_3$): δ 154.88, 151.70, 123.92, 116.23, 113.49, 100.76, 99.41, 87.86, 69.76, 69.56, 31.33, 31.25, 19.31, 19.19, 13.84, 13.81, 0.10.

*Dimethyl 5-((2,5-dibutoxy-4-((trimethylsilyl)ethynyl)phenyl)-ethynyl)isophthalate (**12**).* A flame-dried round-bottom flask was charged with ((2,5-dibutoxy-4-iodophenyl)ethynyl) trimethylsilane (**11**, 1.22 g, 2.75 mmol), diisopropylamine (10 mL), THF (35 mL), CuI (26 mg, 0.137 mmol), dimethyl 5-ethynylisophthalate (**7**, 0.72 g, 3.29 mmol), and $Pd(PPh_3)_2Cl_2$ (0.19 g, 0.275 mmol). The reaction mixture was kept stirring overnight at 40 °C under nitrogen atmosphere, then cooled to room temperature, filtered, and the solvent was removed in vacuo. After standard workup with $CHCl_3$, the crude product was purified by silica gel column chromatography (ethyl acetate:hexane, 1:9, v/v) to give product **12** as a yellow powder (1.24 g; Yield: 84%). MP: 105−106 °C. ^{1}H NMR ($CDCl_3$): δ 8.61 (s, 1H), δ 8.34 (s, 2H), δ 6.96−6.98 (d, 2H, J = 8.0 Hz), δ 3.99−4.03 (m, 4H), δ 3.96 (s, 6H), δ 1.80−1.85 (m, 4H), δ 1.55−1.61 (m, 4H), δ 0.98−1.04 (m, 6H), δ 0.27 (s, 9H) ppm. ^{13}C NMR ($CDCl_3$): δ 165.53, 154.08, 153.62, 136.33, 130.86, 129.92, 124.48, 117.10, 116.85, 114.37, 113.22, 100.90, 100.44, 92.59, 87.83, 69.24, 69.21, 52.45, 31.30, 31.29, 19.28, 19.20, 13.84, 0.14. HRMS (ESI) calcd for $C_{31}H_{38}SiO_6$: 534.7153. Found: 535.2475(M+H).

*Dimethyl 5-((2,5-dibutoxy-4-ethynylphenyl)ethynyl)isophthalate (**13**).* Tetrabutyl-ammonium fluoride trihydrate (1 M in THF, 1.2 mL, 1.2 mmol) in THF (5 mL) was added to a THF (40 mL) solution of dimethyl 5-((2,5-dibutoxy-4-((trimethylsilyl)ethynyl)phenyl) ethynyl)isophthalate (**12**, 0.5 g, 0.94 mmol) at −5 °C (acetone/ice bath). The reaction mixture was stirred at −5 °C for 2 h and monitored by TLC for completion, then quenched by pouring into water. After standard work up with CH_2Cl_2 the crude product was purified by silica gel column chromatography (ethyl acetate:hexane, 1:9, v/v) to give **13** as a yellow powder (0.32 g; Yield: 74%). mp: 128−129 °C. ^{1}H NMR ($CDCl_3$): δ 8.63 (s, 1H), δ 8.36−8.37 (d, 2H, J = 1.5 Hz), δ 7.00−7.01 (d, 2H, J = 5.0 Hz), δ 4.02−4.05 (ddd, 4H, J = 2.5, 6.5 Hz), δ 3.97 (s, 6H), δ 3.37 (s, 1H), δ 1.80−1.87 (m, 4H), δ 1.50−1.63 (m, 4H), δ 0.99−1.04 (m, 6H) ppm. ^{13}C NMR ($CDCl_3$): δ 165.53, 154.08, 153.62, 136.33, 130.86, 129.92, 124.48, 117.10, 116.85, 114.37, 113.22, 100.90, 100.44, 92.59, 87.83, 69.24, 69.21, 52.45, 31.30, 31.29, 19.29, 19.20, 13.84. HRMS (ESI) calcd for $C_{28}H_{30}O_6$: 462.5342. Found: 463.2064(M+H).

*Tetramethyl 5,5′-((([2,2′-bipyridine]-4,4′-diylbis(ethyne-2,1-diyl))-bis(2,5-dibutoxy-4,1-phenylene))bis (ethyne-2,1-diyl))-diisophthalate (**15**).* A flame-dried round-bottom flask was charged with 4,4′-diiodo-2,2′-bipyridine (**14**, 0.12 g, 0.29 mmol), THF (14 mL), triethylamine (2 mL), PPh_3 (15 mg, 0.0588 mmol), dimethyl 5-((2,5-dibutoxy-4-ethynylphenyl)ethynyl) isophthalate (**13**, 0.3 g, 0.65 mmol), and $Pd(PPh_3)_4$ (34 mg, 0.0294 mmol). The reaction mixture was maintained at 50 °C while stirring under nitrogen atmosphere for 4 days, and monitored by TLC for completion. After cooling to room temperature, the reaction mixture was filtered, and the filtrate evaporated in vacuo. After standard workup with $CHCl_3$, the crude product was purified by silica column chromatography (CH_2Cl_2:THF, 9:1, v/v) to give a yellow powder **15** (0.22 g; Yield: 69%). ^{1}H NMR ($CDCl_3$): δ 8.68−8.69 (d, 2H, J = 5.0 Hz), δ 8.63(s, 2H), δ 8.55(s, 2H), δ 8.37−8.38 (d, 4H, J = 1.5 Hz), δ 7.41−7.42 (dd, 2H, J = 1.5, 5.0 Hz), δ 7.05−7.06 (d, 4H, J = 4.0 Hz), δ 4.06−4.09 (t, 8H, J = 6.5 Hz), δ 3.97 (s, 12H), δ 1.85−1.91 (m, 8H), δ 1.59−1.64 (m, 8H), δ 1.03−1.06 (m, 12H) ppm. ^{13}C NMR ($CDCl_3$): δ 165.59, 155.76, 154.00, 153.83, 149.20, 136.43, 132.59, 131.01, 130.08, 125.36, 124.50, 123.17, 117.25, 117.06, 114.29, 113.54, 93.09, 92.50, 90.62, 87.80, 69.48, 69.47, 52.48, 31.35, 19.34, 19.32, 13.89, 13.86. HRMS (ESI) calcd for $C_{66}H_{64}N_2O_{12}$: 1077.2404. Found: 1077.4563.

*Star **YZ3**.* $Ru(DMSO)_4(PF_6)_2$ (12 mg, 0.017 mmol), tetramethyl 5,5′-((([2,2′-bipyridine]-4,4′-diylbis(ethyne-2,1-diyl))bis(2,5-dibutoxy-4,1-phenylene)) bis(ethyne-2,1-diyl))diisophthalate (**15**, 63 mg, 0.058 mmol), THF (4 mL), and nitrogen-purged 1-butanol (4 mL) were added into a round-bottom flask, and the reaction mixture was heated to reflux under nitrogen atmosphere. Every 24 h, the reaction mixture was monitored by UV−vis spectroscopy until the reaction completed. The reaction mixture was cooled to room temperature and filtered. The crude product, a brown powder, was rinsed with acetone and filtered. The filtrate was concentrated in vacuo and addition of hexane resulted in the precipitation of the product as an orange-red powder (**YZ3**, 20 mg; Yield: 34%). ^{1}H NMR (acetone)-d_6: δ 8.98−9.02 (broad, 6H), δ 8.56(s, 6H), δ 8.30(broad, 18H), δ 7.65−7.66 (broad, 6H), δ 7.35 (broad, 6H), δ 7.24−7.25 (broad, 6H), δ 4.14−4.18 (broad, 24H), δ 3.97 (s, 36H), δ 1.85−1.86 (m, 24H), δ 1.59−1.66 (m, 24H), δ 1.01−1.07 (m, 36H) ppm. ^{13}C NMR (acetone)-d_6: δ 164.84, 157.02, 154.43, 153.91, 152.13, 135.67, 133.26, 131.57, 129.68, 129.10, 126.19, 124.26, 117.14, 117.02, 115.49, 112.09, 95.45, 93.33, 90.78, 87.61, 69.28, 69.07, 52.09, 31.31, 31.14, 19.19, 19.05, 13.32, 13.28. HRMS (ESI) calcd for $C_{198}H_{192}N_6O_{36}Ru^{2+}$: 3332.7913. Found: 3332.2478. IR-ATR (cm^{-1}): 2956 ($C-H_{Ar}$), 2873 ($C-H_{CH3}$), 2208 ($C\equiv C$), 1728 ($C=O$), 1605 ($C=C_{Ar}$), 1502, 1438, 1411, 1382, 1355, 1326, 1245 ($C-O$), 1138, 1120, 1105, 1064, 1024, 1002, 9912, 839 ($C-H_{Ar}$).

YZ4 (4). $Ru(DMSO)_4(PF_6)_2$ (56 mg, 0.08 mmol), dimethyl 5-(2,2′-bipyridin-4-ylethynyl)isophthalate (**16**, 0.1 g, 0.28 mmol), THF (5 mL), and nitrogen-purged 1-butanol (12 mL) were added into a round-bottom flask, and the reaction mixture was heated to reflux under nitrogen atmosphere. Every 24 h the reaction mixture was monitored by UV−vis spectroscopy. The reaction mixture was cooled to room temperature and filtered. The resulting powder was rinsed with acetone. The filtrate was evaporated under vacuum and an orange powder (**YZ4**, 78 mg; Yield: 66%) precipitated upon addition of hexane. ^{1}H NMR (acetone)-d_6: δ 8.80(broad, 3H), δ 8.71(broad, 3H), δ 8.65−8.67(m, 3H), δ 8.53(s, 6H), δ 8.24(broad, 3H), δ 7.92−7.93(broad, 3H), δ 7.85−7.86(broad, 3H), δ 7.62−7.63(broad, 3H), δ 7.57−7.58(broad, 3H), δ 4.05(s, 18H). HRMS (ESI) calcd for $C_{66}H_{48}N_6O_{12}Ru^{2+}$: 1218.2103. Found: 1218.2368. The ^{13}C NMR was not available because of the low solubility. IR-ATR (cm^{-1}): 2952 ($C-H_{Ar}$), 2848 ($C-H_{CH3}$), 2217 ($C\equiv C$), 1730 ($C=O$), 1610 ($C=C_{Ar}$), 1476, 1440, 1352, 1319, 1303, 1247 ($C-O$), 1198, 1155, 998, 914, 837 ($C-H_{Ar}$).

RESULTS AND DISCUSSION

Synthesis. The typical method to synthesize homoleptic $Ru(bpy)_3^{2+}$ derivatives involves the reaction between $RuCl_3$ and a bipyridine ligand, followed by treatment with a PF_6^- salt, but when applied to ligands containing OPE moieties, such as the bipyridyl ligands used to prepare Stars YZ1 and YZ2, the reaction led to partially chelated Ru bis(bipyridine) complexes. Thus, the complexation reaction was carried out using $Ru(DMSO)_4(PF_6)_2$, a soluble complex utilized by Otsuki and co-workers.[22] The use of PF_6^- as a noncoordinating anion increases the solubility of Ru polypyridine complexes, which is particularly necessary in the presence of OPE linkers to prevent the precipitation of disubstituted intermediates from the reaction mixture.

In one synthetic approach, shown in Scheme 1, the hexabromosubstituted Ru complex **6** was reacted in a Sonogashira Pd-catalyzed coupling with an excess of linker units. In an alternative approach, shown in Scheme 2, the bpy-linker ligands were synthesized first, followed by the formation of the complex. Both approaches were viable, and the latter approach was preferred when the linker units required several synthetic steps, such as is the case for **15**. The yields of the complex formation ranged from 30 to 66% (i.e., **1** 48%, **2** 30%, **3** 34%, **4** 66%), depending on the solubility of the product and the method used. UV−Vis absorption spectroscopy was employed to monitor the progress of the reaction. A dark brown color indicated the presence of a partially chelated Ru bis(bipyridine) complex, and the appearance of an orange

dx.doi.org/10.1021/ic4004565 | Inorg. Chem. 2013, 52, 7947−7957

Scheme 1. Synthesis of Stars YZ1 and YZ2

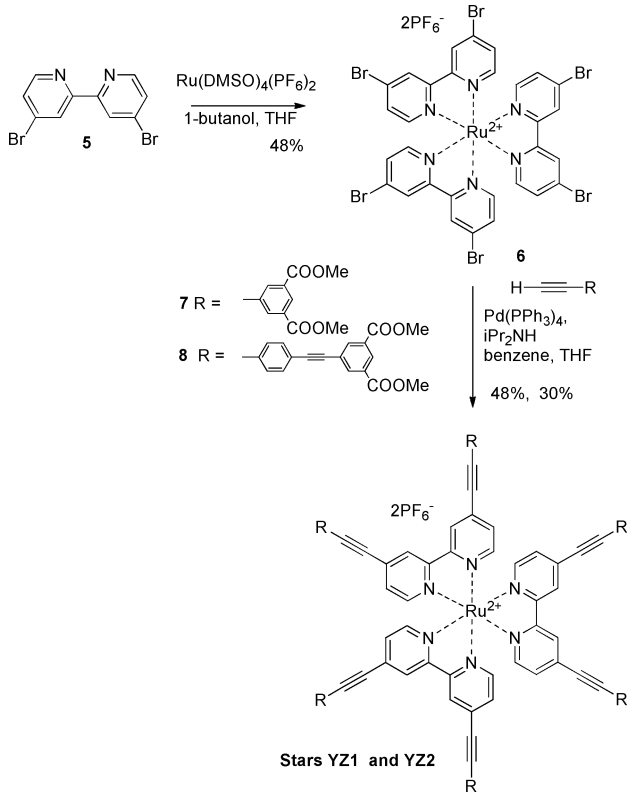

Scheme 2. Synthesis of Stars YZ3 and YZ4

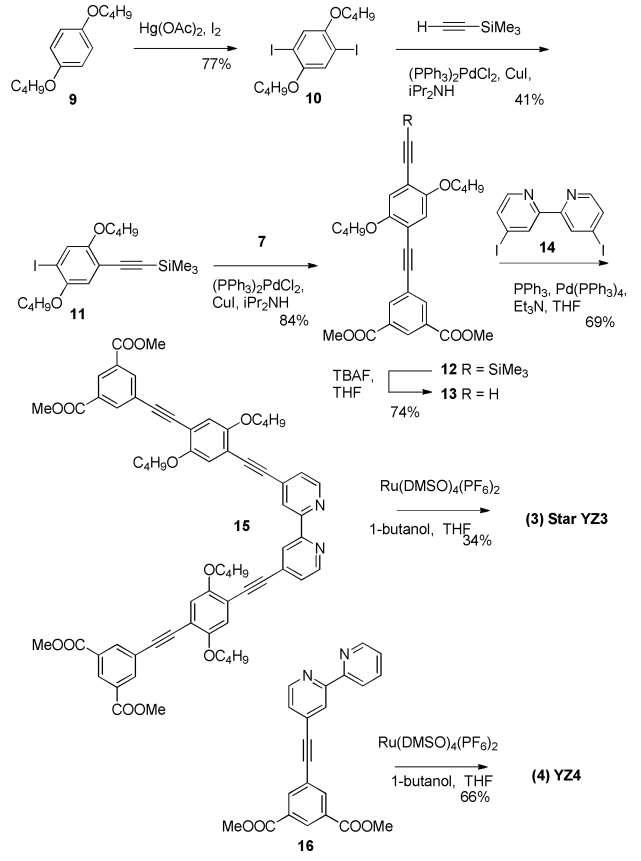

color, typical of the $Ru(bpy)_3^{2+}$ complexes ($\lambda_{MLCT} \sim 450$ nm) indicated the completion of the reaction.

The ligands used to prepare **1** and **2** were synthesized by Pd-catalyzed cross-coupling reactions of the 4,4′-diiodo-2,2′-bipyridine or 4,4′-dibromo-2,2′-bipyridine with linker units **7** or **8** (see Experimental Section). The synthesis of Star YZ3 required the preparation of **15**, a ligand with two *n*-butoxy substituents on the central phenyl ring to improve the solubility. This was prepared as shown in Scheme 2, by iodination of 1,4-dibutoxybenzene to form **10**, which was reacted in a Pd-catalyzed cross coupling reaction with 1 equiv of trimethylsilyl (TMS) acetylene. To obtain prevalently monosubstitution, 1 equiv of TMS acetylene was added dropwise and at low temperature, followed by the catalyst. The reaction mixture was heated to 40 °C. The reaction product, **11**, was coupled with the anchoring unit **7**, and subsequently the TMS group in **12** was deprotected with TBAF to give the terminal alkyne **13**.[19] The disubstituted ligand **15** was obtained in a copper-free Sonogashira coupling reaction with 4,4′-diiodo-2,2′-bipyidine **14** to prevent complexation of Cu(I) salts with the bpy ligand.

Surface Binding. The Star complexes were anchored to metal oxide films following reported procedures.[11,18] The TiO_2 slides were base-pretreated to achieve anchoring between the TiO_2 and the ester groups, consistent with previous work.[23,24] However, the low solubility of Star complexes limited the choice of solvent and concentration range of the solutions and their large size (2 to 4 nm) resulted in lower surface coverage. The nanometer size of the complexes was a concern because the pore necks in mesoporous TiO_2 films can be as small as 3.6−4.2 nm.[25] Indeed, the maximum surface coverage achievable for the four star compounds ($4.4 \pm 2 \times 10^{-8}$ mol cm^{-2}) was considerably lower than the typical sensitizer coverage of the TiO_2 surface, $\sim 1 \times 10^{-7}$ mol cm^{-2}.[26] This is consistent with other reports showing that narrow pore diameters within the TiO_2 nanoparticle thin film can lead to low surface coverages of larger (nm-sized) dyes and coordination compounds.[27,28]

The interfacial surface chemistry that accompanied sensitizer binding was studied through attenuated total reflectance Fourier-transform (ATR-FTIR) spectroscopy (Figure 2 and Supporting Information, Figures S19−S20). Although carboxylic acids are usually preferred for binding, the more soluble carboxylic ester was used to prepare the binding solutions in this study. Our previous work indicated that esters bind to

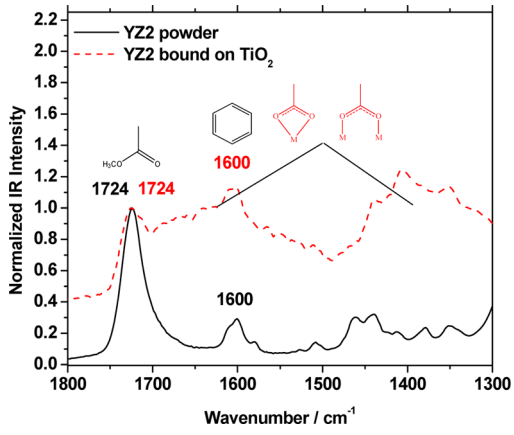

Figure 2. ATR-FTIR spectra of Star YZ2 before (black solid line) and after (red dashed line) binding on TiO_2 films. The overlaid spectra were normalized at the C=O stretching band.

dx.doi.org/10.1021/ic4004565 | Inorg. Chem. 2013, 52, 7947−7957

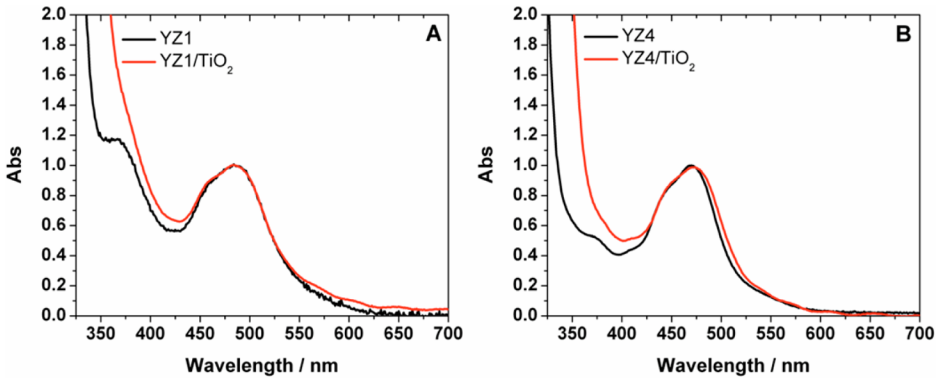

Figure 3. Absorption spectra for (**A**) YZ1 in CH_3CN solution (black) and anchored to base pretreated TiO_2 in neat CH_3CN (red) and (**B**) YZ4 in CH_3CN solution (black) and anchored to base pretreated TiO_2 in neat CH_3CN (red).

Table 1. Room Temperature Photophysical Properties of the Star Complexes in CH_3CN

star	λ_{Abs} (nm) (ε (M^{-1} cm^{-1}))	λ_{PL} (nm)	τ (μs)	ϕ_{PL}	k_r ($\times 10^4$, s^{-1})	k_{nr} ($\times 10^5$, s^{-1})
YZ1	490 (9,800)	645	1.71 ± 0.01	0.072 ± 0.02	4.22	5.52
YZ2[a]	490 (9,800)[a]	650[a]	1.62 ± 0.01[a]	0.038 ± 0.02[a]	2.46[a]	5.97[a]
YZ3[a]	490 (73,800)[a]	640[a]	1.62 ± 0.02[a]	0.12 ± 0.03[a]	7.16[a]	5.51[a]
YZ4	470 (20,100)	635	1.77 ± 0.02	0.068 ± 0.03	3.69	5.40

[a]Data from ref 15.

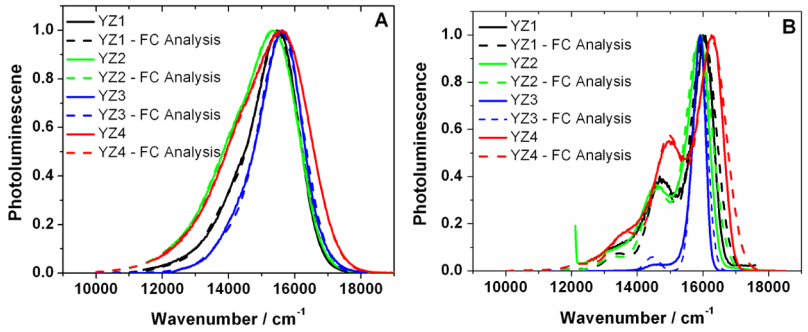

Figure 4. Normalized PL spectra for Stars YZ1, YZ2, YZ3, and YZ4 (**A**) measured in CH_3CN at room temperature and (**B**) measured in a MeOH:EtOH glass at 77 K. Overlaid in dotted lines, for both A and B, are the best fit Franck–Condon line shape analyses.

TiO_2.[12] The spectra of the bound compounds show, a band at ~1610 cm^{-1} ($\nu_{C=C}$) for the phenylene group, and the appearance of broad bands attributed to the mono- and/or bidentate carboxylate linkage (ν1500–1700 cm^{-1}). The presence of unbound ester bands ($\nu_{C=O}$ ~ 1720 cm^{-1}) in the spectra of the Stars/TiO_2 showed that, as expected, not all of the anchoring groups were hydrolyzed to the carboxylate form within the TiO_2 films.

Absorption and Photoluminescence (PL) Spectra in Solution and on Metal Oxide Surfaces. The UV–visible absorption spectra of Stars YZ1 and YZ4 in CH_3CN solutions are shown in Figure 3A and 3B, respectively. The absorption data, as well as the time-dependent density functional theory (TD-DFT) calculations by Persson et al.,[29] for Stars YZ3 and YZ4 were reported previously.[15] The photophysical properties for all Star complexes studied here are summarized in Table 1. Briefly, intense bands in the UV-region at ~300 nm were assigned to the $\pi \rightarrow \pi^*$ transition of the OPE bridges, and a broad metal-to-ligand charge transfer (MLCT) visible absorption was observed near 490 nm. Star YZ3 exhibited an additional absorption band near 400 nm assigned to a $n \rightarrow \pi^*$ transition of the *n*-butoxy substituents[27] and an extinction coefficient at the MLCT absorption maximum $\varepsilon(\lambda_{490})$ = 73,800 which was about an order of magnitude larger than that observed for the other complexes.[15] The UV–visible spectra of the Star complexes YZ1, YZ2, and YZ3 bound to base pretreated TiO_2 (see Experimental Section) did not exhibit any significant changes upon surface attachment, as shown by the overlaid spectra in Figure 3 and previously reported spectra.[15] This was also expected, and suggests that there was no direct contact of the Ru chromophoric unit with the surface. However, a small (~15 nm) red shift was observed for Star YZ4, as shown in Figure 3B. This was expected, as YZ4 lacks octahedral symmetry and is not fully shielded by the linkers from the surface, allowing the Ru core to potentially have a closer proximity to the TiO_2 surface.

Visible light excitation of the Star complexes in fluid solution or in a MeOH:EtOH glass at 77 K resulted in room temperature photoluminescence (PL), Figure 4 A and B, respectively. The PL maximum of Star YZ4 was at slightly higher energy with a significantly sharper band. Pulsed laser excitation of the Star complexes in argon saturated CH_3CN led to exponential PL decays with lifetimes that were longer for Stars YZ1 and YZ4 (1.71 and 1.77 μs, respectively), and slightly shorter for Stars YZ2 and YZ3 (1.62 μs). The rate constant for radiative, k_r, and nonradiative, k_{nr}, decay were derived from the

dx.doi.org/10.1021/ic4004565 | Inorg. Chem. 2013, 52, 7947–7957

Table 2. Photophysical and Electrochemical Properties of Star Complexes YZ1-YZ4

star	YZ1	YZ2	YZ3	YZ4
E_{00} (cm^{-1})[a]	16020	15910	15910	16280
S_M[a]	0.53	0.49	<0.1	0.75
$\Delta\tilde{\nu}_{1/2}$ (cm^{-1})[a]	1000	1000	510	1090
ΔG_{es} (cm^{-1})	16480 (2.04)[b]	16680 (2.07)[b]	16620 (2.06)[b]	17120 (2.12)[b]
$E_{1/2}(Ru^{III/II})$ mV[c]			1560	1400
$E_{1/2}(Ru^{III/II*})$ mV[d]			−520	−760

[a]Data was collected and analyzed at 77 K, except ΔG_{es} (298 K). [b]Value in eV. The $h\omega_M$ (cm^{-1}) values for all the Star complexes were fixed around 1450 cm^{-1}. [c]All measurements were performed in acetonitrile at room temperature under nitrogen atmosphere. Half-wave potentials were reported vs Fc/Fc^+ with experimental error ±20 mV. [d]Excited state reduction potentials, calculated using $E_{1/2}(Ru^{III/II*}) = E_{1/2}(Ru^{III/II}) - \Delta G_{es}$.

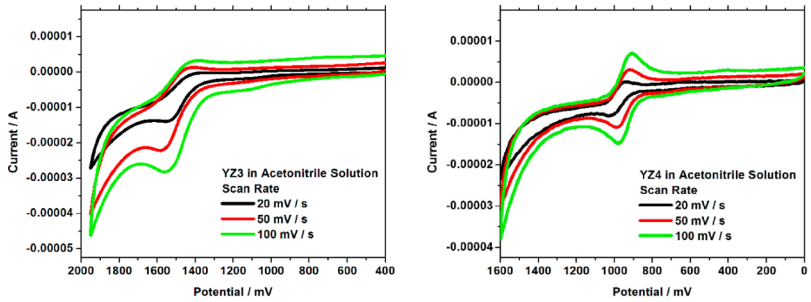

Figure 5. Cyclic voltammograms of Star YZ3 (left) and Star YZ4 (right) in 0.26 M tetrabutylammonium hexafluorophosphate CH_3CN vs Fc/Fc^+ measured at the indicated scan rates.

experimentally determined lifetimes $1/\tau = (k_r + k_{nr})$ and the quantum yield of photoluminescence $\phi_{PL} = k_r/(k_r + k_{nr})$, see Table 1. The rate constants suggest that the enhanced PL quantum yield for YZ3 results from a more favorable radiative rate constant.[30]

Franck–Condon (FC) Line Shape Analysis. To obtain more information about the free energy difference (ΔG_{es}), between the excited and ground states, the photoluminescence spectra at room temperature and at 77 K were analyzed using a Franck–Condon (FC) line shape analysis, Figure 4. The corrected PL spectra, measured in nm, were converted to units of energy ($\tilde{\nu}$) by the methods described by Parker and Reese.[31] The analysis is based on a single-mode line shape analysis of the PL spectra with eq 1,

$$I(\tilde{\nu}) = \sum_{\nu_m}^{5}\left[\left(\frac{E_{00} - \nu_m\cdot\hbar\cdot\omega_m}{E_{00}}\right)^3\cdot\frac{S_M^{\nu_m}}{\nu_m!}\cdot \exp\{-4\ln 2[(\tilde{\nu} - E_{00} + \nu_m\cdot\hbar\cdot\omega_m)/\Delta\tilde{\nu}_{1/2}]^2\}\right] \quad (1)$$

where E_{00} is the maximum energy of the first medium frequency mode, $h\omega_M$ (cm^{-1}), S_M is the Huang–Rhys factor, $\Delta\tilde{\nu}_{1/2}$ is the full-width at half-maximum of the medium-frequency progression, and ν_M is the vibrational quantum number for the medium frequency acceptor mode which was set to five.[32,33] In this analysis, $h\omega_M$ was constrained to be 1450 cm^{-1} which represent an average vibrational acceptor mode.[34] Best fits of the spectral data to eq 1 yielded the E_{00}, S_M, and $\Delta\tilde{\nu}_{1/2}$ values given in Table 2. From the $\Delta\tilde{\nu}_{1/2}$ and E_{00} parameters, the Gibbs free energy stored in the MLCT excited state, ΔG_{es}, was calculated from eq 2.[34,35]

$$\Delta G_{es} = E_{00} + \frac{(\Delta\tilde{\nu}_{1/2})^2}{16k_BT\ln(2)} \quad (2)$$

Table 2 reveals striking changes in $\Delta\tilde{\nu}_{1/2}$ and S_M for the different compounds. The former was obvious from the raw experimental data shown in Figure 4. The approximately factor of 3 decrease in the electron-vibrational coupling constant, S_M, between Star YZ2 and Star YZ3 is consistent with the previously described notion that the electron-donating butoxy (*n*-BuO) groups on the OPE linkers in Star complex YZ3 enhances mixing of the MLCT state and the π–π^* state of the OPE spacer.[36] Complex YZ4 has three less OPE bridges, a property which impacts the Huang–Rhys factors in the form of a larger S_M value. The free energy stored in the excited states was derived from room temperature data and was very similar for the four compounds (~ 2.08 eV).

Electrochemistry. Cyclic voltammetry (CV) data of Stars YZ3 and YZ4 at different scan rates in acetonitrile solution with tetrabutylammonium hexafluorophosphate (0.2 M) electrolyte are shown in Figure 5. Star YZ4 displayed quasi-reversible $Ru^{III/II}$ waves and Star YZ3 displayed irreversible redox chemistry. The redox wave was quasi-reversible as the anodic and cathodic peak currents were approximately equal, but the peak-to-peak separation was greater than 100 mV. For Star YZ3, the oxidation current was larger than the reduction. Both Star complexes showed an additional irreversible oxidation at more positive potentials. An interesting observation is the larger peak-to-peak separation in the CV of Star YZ3, the complex having the Ru center surrounded by OPE linkers substituted with *n*-butoxy chains, compared to YZ4, the complex with the Ru center "exposed" to the solvent. One possible explanation is that the more reversible behavior for YZ4 results from faster redox kinetics brought about by a closer approach of the Ru center with the electrode surface. Because of their low solubility, the cyclic voltammograms of Stars YZ1 and YZ2 were not obtained. The electrochemical data for star complexes (vs Fc/Fc^+) in acetonitrile solution are reported in Table 2.

When compared to the ground state $E_{1/2}(Ru^{III/II})$ reduction potential value of $Ru(bpy)_3^{3+/2+}$ (1260 mV) and of previously

dx.doi.org/10.1021/ic4004565 | Inorg. Chem. 2013, 52, 7947–7957

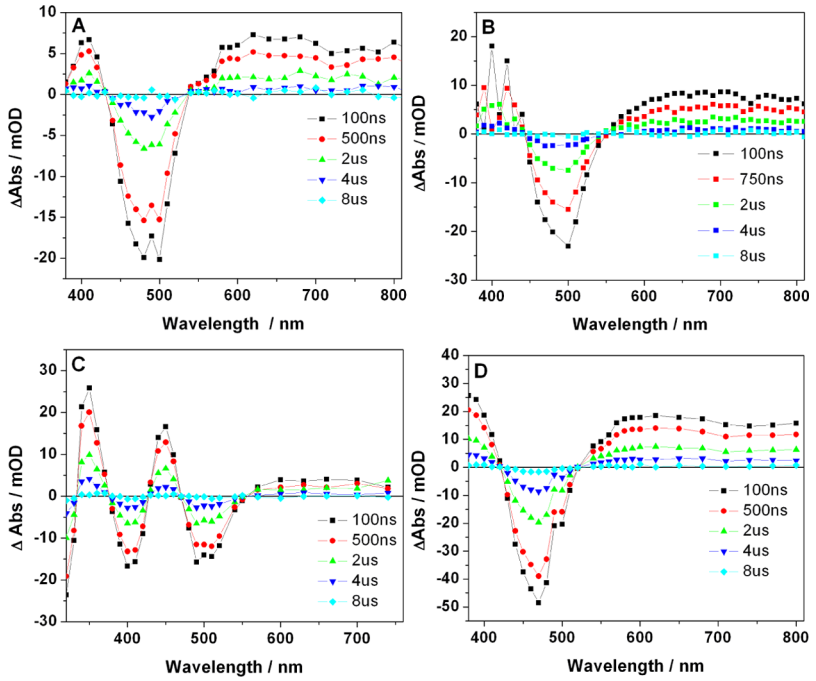

Figure 6. Transient absorption difference spectra recorded at the indicated delay times after pulsed 532 nm light (8 ns fwhm, 2 mJ/cm^2) excitation of the indicated Star complexes in CH_3CN solution. (A) Star YZ1, (B) Star YZ2, (C) Star YZ3, and (D) Star YZ4.

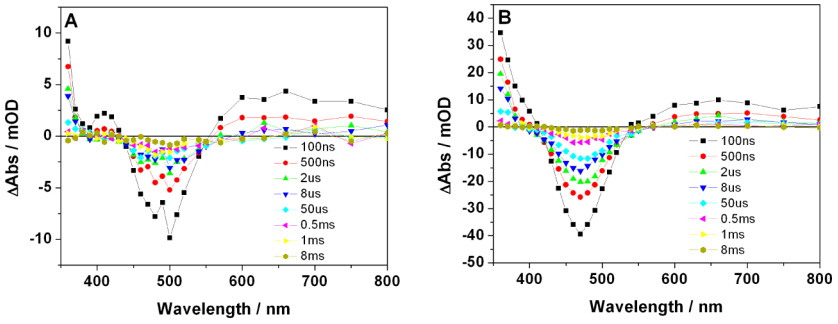

Figure 7. Transient absorption difference spectra recorded at the indicated delay times after pulsed 532 nm light (8 ns fwhm, 2 mJ/cm^2) excitation of the indicated Star complexes anchored to TiO_2 in 0.2 M $LiClO_4/CH_3CN$ solution. (A) YZ1/TiO_2, (B) YZ4/TiO_2.

reported heteroleptic Ru(bpy)$_2$Ipa rigid-rods (1300 mV) that possess one bpy ligand substituted with a single OPE linker,[14] the $E_{1/2}$ value of Star YZ3 (1560 mV) and Star YZ4 (1400 mV) were shifted to more positive potentials. The excited state reduction potentials of the ruthenium Star complexes (−520 mV for Star YZ3 and −760 mV for StarYZ4) were less negative than such reference sensitizers. Because of solubility and surface coverage issues it was not possible to determine the redox potentials for YZ1 and YZ2; however, the excited state reduction potentials were estimated to be −560 mV vs Fc/Fc$^+$.[14] Nevertheless, the excited state reduction potentials for YZ1−YZ4 are considerably more negative than the onset of TiO_2 reduction measured electrochemically and spectroelectrochemically, indicating that excited state injection for such complexes is thermodynamically favored.[37,38]

Excited State Absorption Spectra in Solution and Bound. The excited states of the Star complexes were studied by nanosecond transient absorption spectroscopy, Figure 6. The difference spectra measured after pulsed 532 nm excitation of the four Star complexes in fluid acetonitrile solution were consistent with those previously reported for similar compounds.[14] Clean isosbestic points were observed, and the first-order excited state relaxation kinetics were wavelength independent with abstracted lifetimes that were in good agreement with those determined from time-resolved PL measurements.

A long-lived transient was observed when a large excess of $LiClO_4$ (0.05 M) was present in Star YZ3 acetonitrile solutions, Supporting Information, Figure S22. The addition of $LiClO_4$ also resulted in the formation of an orange precipitate. The origin(s) of this behavior is unknown, but lithium ion coordination to ester functional groups of ruthenium polypyridyl compounds has been previously reported, and this may result in aggregation and/or precipitation of the complexes.[34]

Pulsed laser excitation of the Star complexes anchored to TiO_2 and immersed in 0.2 M $LiClO_4$ acetonitrile solution resulted in the appearance of absorption spectra that were predominately due to the MLCT excited state, Figure 7. At longer observation times, > 10 μs, small absorption features were observed whose spectra and kinetics clearly did not derive from the excited state. By analogy to other sensitized thin films, the longer lived transient was assigned to an interfacial charge separated state composed of an electron injected into TiO_2 and

dx.doi.org/10.1021/ic4004565 | Inorg. Chem. 2013, 52, 7947−7957

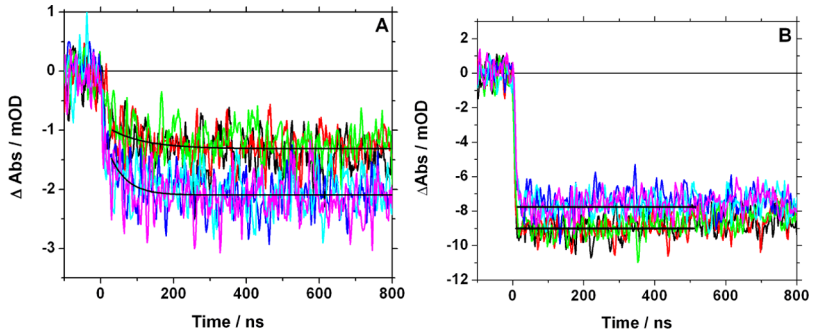

Figure 8. Transient absorption changes monitored at 442 nm after pulsed 532 nm light excitation of Star/TiO_2 thin films in a 0.2 M $LiClO_4$/CH_3CN solution at fluences of (A) YZ1 at 3.7 and 7 mJ cm^{-2}, (B) YZ4 at 4.5 and 7.0 mJ cm^{-2}. Overlaid are fits to a first-order kinetic model, k_{obs} = 3.7 × 10^7 s^{-1} for YZ1/TiO_2, and the injection rate constant could not be time-resolved for YZ4/TiO_2.

the oxidized Star complex.[39] The weak absorption in the red was assigned to the injected electron while the long-lived bleach results from the fact that the oxidized Ru complexes absorb less light than the ground state. The positive absorption observed at 450 nm has previously been reported for related compounds, and its coincidence with an absorption feature observed after electrochemical oxidation led to its assignment as a ligand-to-metal charge transfer transition.[14]

Charge Injection and Recombination on TiO_2 Thin Films. The quantum yields for excited state injection were measured by comparative actinometry with $Ru(bpy)_3^{2+}$ thin films as was previously described[39] and with a Ru-$(dcb)_2(NCS)$/TiO_2 thin film where an injection yield of unity was assumed. The injection yields were measured on a 10 ns time scale at the 410 nm isosbestic point. The data for multiple samples of YZ1/TiO_2, YZ2/TiO_2, and YZ4/TiO_2 were consistent with an injection yield, $\varphi_{inj} \leq 0.14$. Measurements of the injection yield for YZ3/TiO_2 were complicated by shifts of the isosbestic points when $LiClO_4$ was present in the acetonitrile. Nevertheless, comparative studies in which equal number of photons were absorbed indicated that the injection yield for YZ3/TiO_2 was <0.01.

For the Star complexes anchored to TiO_2, excited state injection occurs in the presence of long-lived excited states, and overlapping absorption bands in the visible region require observation at isosbestic points. At isosbestic points the excited state and the ground state absorb light equally which enables excited state injection and charge recombination to be cleanly monitored. Such data was obtained for multiple samples of YZ1/TiO_2 and YZ4/TiO_2 compound at three separate laser fluencies, Figure 8. In the case of YZ1/TiO_2, a laser fluency independent exponential rise of the absorption was observed consistent with the appearance of the oxidized sensitizer and hence corresponded to excited state injection. Analysis of this data with a first order kinetic model revealed an excited state injection rate constant of k_{inj} = 3.5 ± 0.1 × 10^7 s^{-1} for YZ2/TiO_2,[15] and k_{inj} = 3.7 ± 0.1 × 10^7 s^{-1} for YZ1/TiO_2. Interestingly, charge injection could not be time-resolved after light excitation of YZ4/TiO_2 indicating that $k_{inj} > 10^8$ s^{-1}. This implies that the symmetric Star motif is required to prevent close contact with the TiO_2 surface.

The injection rate constant can also be calculated from the measured injection quantum yield and the radiative and nonradiative rate constants measured in fluid solution, eq 3. An injection rate constant of $k_{inj,calc}$ = 3.0 × 10^5 s^{-1} was thus calculated. This value is about two

$$\phi_{inj} = \frac{k_{inj}}{k_{inj} + k_r + k_{nr}} \quad (3)$$

orders of magnitude smaller than the experimentally measured value. The discrepancies between the calculated and experimental injection time scales can be explained either by a change in k_r and/or k_{nr} upon surface binding or heterogeneity in the TiO_2 acceptor states. This latter explanation is supported by previous single molecule spectroscopic data reported by Xie and Liu, who found a broad range of injection rates on a planar metal oxide surface.[40] While one would anticipate that both k_r and k_{nr} would change from their solution values upon surface binding, 2 orders of magnitude seems too large. Therefore, it appears that under these conditions a small fraction of unique acceptor states are present in TiO_2 anatase nanocrystallites that can rapidly accept electrons that are ≥10 Å away.

Charge recombination was sufficiently slow that it could be monitored on time scales longer than excited state decay, as shown in Figure 9. The observed kinetics were nonexponential but were well described by the Kohlrausch–Williams–Watts (KWW) function, eq 4.[41]

$$I = I_0 \exp[-(k_{obs} \cdot t)^{\beta}] \quad (4)$$

The reciprocal of the first moment of the KWW function was taken as an average value for charge recombination, and the k_{cr} values that were abstracted from this data are presented in Table 3. Interestingly, even with increased laser fluency, because of the low quantum yield of injection and instrument sensitivity, the charge recombination was not complete until

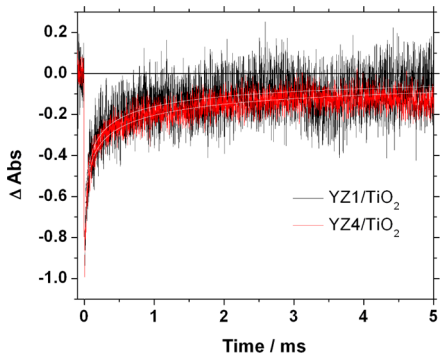

Figure 9. Normalized absorption changes measured after pulsed light (532 nm, 7 mJ cm^{-2}) excitation of YZ1/TiO_2 (black) and YZ4/TiO_2 (red). Overlaid on the data are best fits to the Kohlrausch–Williams–Watts (KWW) function.

dx.doi.org/10.1021/ic4004565 | Inorg. Chem. 2013, 52, 7947–7957

Table 3. Room Temperature Photophysical and Charge Separation/Recombination Properties of StarsYZ1−YZ4 Anchored to TiO_2

sensitized film	λ_{Abs} (nm)	λ_{PL} (nm)	ϕ_{inj}	k_{inj} (s^{-1})	k_{cr} (s^{-1})[a]
YZ1/ TiO_2	490	650	0.07 ± 0.01	3.7×10^7	$7.4 \pm 5 \times 10^2$
YZ2/ TiO_2	490	655	0.04 ± 0.01	[b]3.5×10^7	$1.6 \pm 1 \times 10^2$
YZ3/ TiO_2	490	655	<0.01	*c*	[c]$0.8 \pm 2 \times 10^2$
YZ4/ TiO_2	470	650	0.14 ± 0.01	$>10^8$	$3.4 \pm 4 \times 10^2$

[a]A representative charge recombination rate constant, k_{cr}, was taken as the first moment of the KWW function, were β was held at 0.20. [b]From reference 15. [c]The small amplitude of the absorption transient precluded kinetic analysis of the injection rate constant and led to greater uncertainty in the charge recombination rate constant.

~100 ms, and there was still a noticeable population of charge separated states after 5 ms, see Figure 9. The time scale for charge recombination was much slower than what has been shown in our own or other research groups.[1] It can therefore be concluded that the larger, nanosized, Star complexes are very effective at inhibiting charge recombination.

CONCLUSION

In conclusion, four homoleptic star-shaped ruthenium polypyridyl complexes, Star YZ1, Star YZ2, Star YZ3, and Star YZ4, the latter having three identical bpy ligands carrying rigid OPE linker units, with and without *n*-butoxy chains, and terminating with an isophthalic ester, were synthesized by two different approaches, both involving a sequence of Pd-catalyzed cross coupling and complexation reactions. The Star complexes were studied by steady-state and time-resolved spectroscopy, electrochemistry and IR in solution and when anchored to mesoporous TiO_2 nanocrystalline thin films. The results suggest that the highly symmetric arrangement of long, rigid spacers between the bpy ligand and the surface anchoring groups isolate the sensitizer unit from the surface, resulting in slower excited state injection and slower charge recombination. Notably, slower interfacial charge transfer was achieved through synthetic design, by the use of ligand spacers, and not through surface blocking layers on TiO_2.[42] In addition, there was no evidence of hole transfer, or triplet−triplet annihilation between neighboring Star complexes on TiO_2 suggesting no intermolecular excited state or oxidized state interactions. The absorption and photoluminescence properties of the Star complexes were unperturbed upon surface binding, and the addition of *n*-butoxy groups on the OPE spacers dramatically increased the extinction coefficient and radiative rate constant of the complexes. Thus the use of homoleptic star complexes is a viable strategy to isolate sensitizers from highly heterogeneous semiconductor surfaces to achieve control of injection/charge recombination time scales, and to minimize sensitizer-sensitizer interaction. Unfortunately, excited state injection was slowed to the point that nonradiative relaxation was competitive, and the injection yields were thus low precluding practical application of these Star complexes in DSSCs. This level of interfacial charge transfer control however is potentially of interest for the design of OLEDs, where it is important to *block unwanted excited state quenching reactions* that occur with other molecules or the metal oxide surface. The complexes are also of interest to enhance our fundamental understanding of the TiO_2/sensitizer interface in DSSCs. In fact, the influence of the nature of varying bridges and/or anchor groups of Star complexes on interfacial charge transfer is being studied computationally[29] and experimentally.[13] In particular, current work includes the development of star complexes that exhibit increased electronic coupling to TiO_2 through 1,2,3-triazole-containing bridges.[13]

ASSOCIATED CONTENT

Supporting Information

^1H and ^{13}NMR spectra of YZ1-YZ4 and their synthetic precursors, synthetic scheme for the bipyridyl ligands for Stars YZ1 and YZ2, absorption spectra and IR spectra of YZ1−YZ4 and in solution and bound, transient absorption difference spectra of YZ4 in the presence of $LiClO_4$. This material is available free of charge via the Internet at http://pubs.acs.org.

AUTHOR INFORMATION

Corresponding Author

*E-mail: galoppin@rutgers.edu (E.G.), meyer@jhu.edu (G.J.M).

Notes

The authors declare no competing financial interest.

ACKNOWLEDGMENTS

The Division of Chemical Sciences, Geosciences and Biosciences Division, Office of Basic Energy Sciences, Office of Science, U.S. Department of Energy DE-FG02-01ER15256 (E.G.) and DE-FG02-96ER14662 (G.J.M.) is gratefully acknowledged for research support.

REFERENCES

(1) Ardo, S.; Meyer, G. J. *Chem. Soc. Rev.* **2009**, *38*, 115−164.
(2) Reynal, A.; Palomares, E. *Eur. J. Inorg. Chem.* **2011**, *2011*, 4509−4526.
(3) Hagfeldt, A.; Boschloo, G.; Sun, L.; Kloo, L.; Pettersson, H. *Chem. Rev.* **2010**, *110*, 6595−6663.
(4) Mishra, A.; Fischer, M. K. R.; Bäuerle, P. *Angew. Chem., Int. Ed.* **2009**, *48*, 2474−2499.
(5) Galoppini, E. *Coord. Chem. Rev.* **2004**, *248*, 1283−1297.
(6) Ernstorfer, R.; Gundlach, L.; Felber, S.; Storck, W.; Eichberger, R.; Willig, F. *J. Phys. Chem. B* **2006**, *110*, 25383−25391.
(7) Yella, A.; Lee, H.-W.; Tsao, H. N.; Yi, C.; Chandiran, A. K.; Nazeeruddin, M. K.; Diau, E. W.-G.; Yeh, C.-Y.; Zakeeruddin, S. M.; Grätzel, M. *Science* **2011**, *334*, 629−634.
(8) Hannappel, T.; Burfeindt, B.; Storck, W.; Willig, F. *J. Phys. Chem. B* **1997**, *101*, 6799−6802.
(9) Chang, C.-W.; Luo, L.; Chou, C.-K.; Lo, C.-F.; Lin, C.-Y.; Hung, C.-S.; Lee, Y.-P.; Diau, E. W.-G. *J. Phys. Chem. C* **2009**, *113*, 11524−11531.
(10) Gundlach, L.; Ernstorfer, R.; Willig, F. *J. Phys. Chem. C* **2007**, *111*, 13586−13594.
(11) Thyagarajan, S.; Galoppini, E.; Persson, P.; Giaimuccio, J. M.; Meyer, G. J. *Langmuir* **2009**, *25*, 9219−9226.
(12) Zhang, Y.; Galoppini, E.; Johansson, P. G.; Meyer, G. J. *Pure Appl. Chem.* **2011**, *83*, 861−868.
(13) Chitre, K. P.; Guillén, E.; Yoon, A. S.; Galoppini, E. *Eur. J. Inorg. Chem.* **2012**, *2012*, 5461−5464.
(14) Wang, D.; Mendelsohn, R.; Galoppini, E.; Hoertz, P. G.; Carlisle, R. A.; Meyer, G. J. *J. Phys. Chem. B* **2004**, *108*, 16642−16653.
(15) Johansson, P. G.; Zhang, Y.; Abrahamsson, M.; Meyer, G. J.; Galoppini, E. *Chem. Commun.* **2011**, *47*, 6410−6412.
(16) O'Donnell, R. M.; Johansson, P. G.; Abrahamsson, M.; Meyer, G. J. *Inorg. Chem.* **2013**, *52* (12), 6839−6848.

(17) Heimer, T. A.; D'Arcangelis, S. T.; Farzad, F.; Stipkala, J. M.; Meyer, G. J. *Inorg. Chem.* **1996**, *35*, 5319−5324.
(18) Thyagarajan, S.; Liu, A.; Famoyin, O. A.; Lamberto, M.; Galoppini, E. *Tetrahedron* **2007**, *63*, 7550−7559.
(19) Adams, C. J.; Bowen, L. E.; Humphrey, M. G.; Morrall, J. P. L.; Samoc, M.; Yellowlees, L. J. *Dalton Trans.* **2004**, *24*, 4130−4138.
(20) Kavanagh, P.; Leech, D. *Tetrahedron Lett.* **2004**, *45*, 121−123.
(21) Wang, D.; Schlegel, J. M.; Galoppini, E. *Tetrahedron* **2002**, *58*, 6027−6032.
(22) Otsuki, J.; Hiroyuki, K.; Sota, T.; Hiroshi, S.; Toshio, T. *Chem. Lett.* **2002**, *31*, 610−611.
(23) Qu, P.; Meyer, G. J. *Langmuir* **2001**, *17*, 6720−6728.
(24) Heuer, W. B.; Xia, H.-L.; Abrahamsson, M.; Zhou, Z.; Ardo, S.; Sarjeant, A. A. N.; Meyer, G. J. *Inorg. Chem.* **2010**, *49*, 7726−7734.
(25) Vargas-Florencia, D.; Edvinsson, T.; Hagfeldt, A.; Furo, I. *J. Phys. Chem. C* **2007**, *111*, 7605−7611.
(26) Staniszewski, A.; Morris, A. J.; Meyer, G. J. *J. Phys. Chem. B* **2007**, *111*, 6822−6828.
(27) Nejati, S.; Lau, K. K. S. *Nano Lett.* **2011**, *11*, 419−423.
(28) Fan, S.-Q.; Kim, C.; Fang, B.; Liao, K.-X.; Yang, G.-J.; Li, C.-J.; Kim, J.-J.; Ko, J. *J. Phys. Chem. C* **2011**, *115*, 7747−7754.
(29) Persson, P.; Knitter, M.; Galoppini, E. *RSC Adv.* **2012**, *2*, 7868−7874.
(30) Bowen, E. J.; Wokes, F. *Fluorescence of Solutions*; Longmans Green & Co: London, U.K., 1953.
(31) Parker, C. A.; Rees, W. T. *Analyst* **1960**, *85*, 587−600.
(32) Caspar, J. V.; Meyer, T. J. *J. Am. Chem. Soc.* **1983**, *105*, 5583−5590.
(33) Heimer, T. A.; Bignozzi, C. A.; Meyer, G. J. *J. Phys. Chem.* **1993**, *97*, 11987−11994.
(34) Worl, L. A.; Duesing, R.; Chen, P.; Ciana, L. D.; Meyer, T. J. *J. Chem. Soc., Dalton Trans.* **1991**, 849−858.
(35) Kober, E. M.; Caspar, J. V.; Lumpkin, R. S.; Meyer, T. J. *J. Phys. Chem.* **1986**, *90*, 3722−3734.
(36) Chaignon, F.; Torroba, J.; Blart, E.; Borgstrom, M.; Hammarström, L.; Odobel, F. *New J. Chem.* **2005**, *29*, 1272−1284.
(37) Morris, A. J.; Meyer, G. J. *J. Phys. Chem. C* **2008**, *112*, 18224−18231.
(38) Bisquert, J.; Fabregat-Santiago, F.; Mora-Seró, I.; Garcia-Belmonte, G.; Barea, E. M.; Palomares, E. *Inorg. Chim. Acta* **2008**, *361*, 684−698.
(39) Bergeron, B. V.; Kelly, C. A.; Meyer, G. J. *Langmuir* **2003**, *19*, 8389−8394.
(40) Liu, H. P.; Xie, X. S. *J. Phys. Chem. B* **1997**, *101*, 2753−2757.
(41) Williams, G.; Watts, D. C. *Trans. Faraday Soc.* **1970**, *66*, 80−85.
(42) Palomares, E.; Clifford, J. N.; Haque, S. A.; Lutz, T.; Durrant, J. R. *J. Am. Chem. Soc.* **2002**, *125*, 475−482.

■ NOTE ADDED AFTER ASAP PUBLICATION

Due to a production error, this paper was published on the Web on June 24, 2013, with errors in equation 1. The corrected version was reposted on June 26, 2013.